Two Novel Inorganic-Organic Hybrid Frameworks Based on In^{III}-BTC and In^{III}-BTEC

Zheng-Zhong Lin,[a] Fei-Long Jiang,[a] Lian Chen,[a] Da-Qiang Yuan,[a] You-Fu Zhou,[a] and Mao-Chun Hong*[a]

Keywords: Indium(III) / Benzenemulticarboxylate

Hydrothermal reactions of $InCl_3$ with 1,3,5-benzenetricarboxylic acid (H_3BTC) or pyromellitic dianhydride produced $[In_2(BTC)_2(H_2O)_2]_n \cdot 2nH_2O$ (**1**) and $[In_2(H_2BTEC)_2(OH)_2]_n \cdot 2nH_2O$ (**2**), respectively (H_4BTEC = 1,2,4,5-benzenetetracarboxylic acid). The structure of **1** is a 2D double-layer network, while that of **2** is a 3D framework constructed from chains of corner-linked octahedra. Intense greenish-blue emissions at 494 nm (λ_{ex} = 325 nm) for **1** and 489 nm (λ_{ex} = 337 nm) for **2** were observed in the solid state.

Introduction

The development of organic-inorganic hybrid compounds constructed by the deliberate selection of metals and multifunctional exodentate ligands represents one of the most active research area in chemistry. The fascinating structures of these complexes together with their functional properties makes them highly prospective as a new class of materials.[1−4] 1,3,5-benzenetricarboxylic acid (H_3BTC) and 1,2,4,5-benzenetetracarboxylic acid (H_4BTEC) are two promising ligands which provide high symmetry, diverse charge and a multi-connecting ability which has been applied in the design of hybrid complexes exploiting both the diversity of metal coordination geometries and weak intermolecular forces such as π−π interactions and hydrogen bonding. The rigid conformation and strong coordinating ability of the carboxylate groups bestows excellent thermal properties on the resultant hybrid complexes. The use of H_3BTC and divalent metal ions has led to the generation of products consisting 1D chains,[5,6] 2D layers[7−11] and 3D structural frameworks.[12−16] H_4BTEC is a building block that has been commonly adopted in the design of hybrids in connection with transition[17−21] and rare earth metal elements.[22−24] In the search for a further class of hybrid materials we have introduced a trivalent metal, namely indium(iii), in order to investigate the influence of a change in the metal centre on the coordination architecture during the course of the assembly of the metal centres with H_3BTC or H_4BTEC. It was postulated that the incorporation of trivalent metal ions might create diverse structures different from those containing divalent metal ions because of the increased valence charge. Furthermore, compared with the systematic and extensive studies on M^{II}-BTC complexes, reports of M^{III}-BTC complexes are rare.[25,26] Although some literature reports concerning M^{III}-BTEC complexes have recently appeared, the metal centres incorporated were mostly confined to the rare earth metal elements,[23,24] Fe^{III} [27] or V^{III}.[28] There is a deficiency of the selection of the ^{III}A group elements as inorganic linkers. We addressed this situation by choosing In^{III} as the metal and a series of 3D In^{III}-BTC and 3D In^{III}-BTEC complexes with protonated pyridine or pyridine derivatives as templates and counter anions have been synthesised. Herein we describe a 2D double-layered In^{III}-BTC compound $[In_2(BTC)_2(H_2O)_2]_n \cdot 2nH_2O$ (**1**) and a 3D In^{III}-BTEC compound $[In_2(H_2BTEC)_2(OH)_2]_n \cdot 2nH_2O$ (**2**) showing characteristic $In^{III}O_4(OH)_2$ octahedral chains.

Results and Discussion

The formation of compounds **1** and **2** was found to be extremely sensitive to the pH value of the reaction mixture. Synthetic studies were carried out using pyridine as a basic reagent to adjust the pH value in the reaction system. In both systems, a pH value between 2 and 3 is an essential condition for the formation of **1** and **2**. For the preparation of In^{III}-BTC, a pH value ranging from 3 to 4 produces a mixture of **1** and a 3D porous coordination polymeric compound.[29] Likewise, two phases (compound **2** and a 3D porous In^{III}-BTEC framework[30]) also crystallise concurrently from the reaction system of **2** when a pH value of 3−4 is maintained. In both reaction systems, more basic pH values led to predominant formation of the 3D porous by-prod-

[a] State Key Laboratory of Structural Chemistry, Fujian Institute of Research on the Structure of Matter, Chinese Academy of Sciences, Graduate School of the Chinese Academy of Sciences, Fujian, Fuzhou, 350002, China
Fax: (internat.) +86-591-3714946
E-mail: hmc@ms.fjirsm.ac.cn, zzlin@ms.fjirsm.ac.cn

ucts. Furthermore, when the reactions were carried out without pyridine as a basic reagent, the yields of **1** and **2** were very low. Thus, to ensure a high yield of **1** and **2**, an appropriate amount of pyridine is needed to adjust the pH value around 3.

Compound **1** exhibits a double-layer sheet configuration (Figure 1) generated from the interconnection of two single-layers which are produced from the extension of honeycomb-like grids along the (100) plane. Three In^{III} centres and three BTC trianions form such a 6-membered grid with dimensions of about 7.4 Å × 9.2 Å. Inside the grids, each indium atom binds to six carboxylate oxygen atoms from four BTC groups and one water oxygen atom (O7) to form a slightly distorted pentagonal bipyramidal motif. The dihedral angle between the benzene plane of the BTC group and the plane defined by In, InA, and InB is about 12.6°. Consequently, the sheet adopts a slightly wavy configuration. A bidentate carboxylate arm (C9−O5−O6) lies out of the BTC benzene ring plane with a dihedral angle as high as 26° such that the carboxylate arms act as the bridges linking two single-layers into a double-layer. The other two carboxylate arms bond in a chelating bidentate mode and participate in the propagation of the grids. The two single-layers are related to each other through the twofold screw symmetry operation and the distance between them is about 3.8 Å. Because of the translation operation of the screw axis, the available sizes of honeycomb-like grids are significantly reduced. This explains the fact that **1** absorbs little nitrogen gas even after dehydration.[31] To balance the charge, O7 can be considered to be a coordinated water oxygen atom. This assumption is confirmed by bond valence calculations for O7 which give a result of 0.5.[32] The

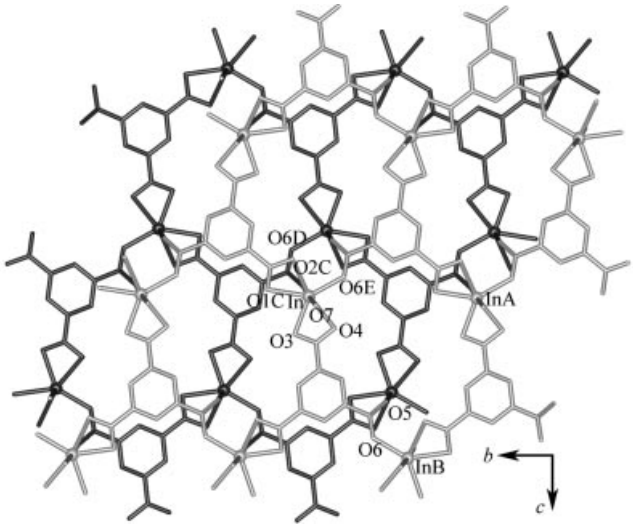

Figure 1. View of the double-layer in **1** interlinked by two single-layers displayed in black and light grey, respectively; free water and coordinated water molecules are not shown for clarity; selected bond lengths (Å): In−InA 8.979(1); In−InB 10.288(1); InA−InB 9.468(1); In−O7 2.167(3); In−O3 2.198(1); In−O4 2.292(1); In−O1C 2.271(3); In−O2C 2.304(4); In−O5D 2.138(5); In−O6E 2.144(3); selected bond angles (°): O7−In−O5D 178.0(1); O3−In−O7 89.0(1); O1C−In−O7 95.6(1); symmetry code: (A) x, $1 + y$, z (B) x, $1.5 - y$, $0.5 + z$ (C) x, $0.5 - y$, $-0.5 + z$ (D) $-x$, $-0.5 + y$, $0.5 - z$ (E) x, $1.5 - y$, $-0.5 + z$

In−O7 vectors are perpendicular to the double-layer plane and point towards the extra double-layer region. Furthermore, the double-layers are stacked in parallel separated by about 4 Å. This is sufficiently close such that the In−O7 vectors on the double-layers are interdigitated. Coordinated water oxygen atoms form strong hydrogen bonds with carboxylate oxygen atoms from adjacent double-layers [O7···O2A, 2.775(4) Å, (A):$1 - x$, $0.5 + y$, $0.5 - z$]. The free water molecules included in the honeycomb-like grids also form hydrogen bonds with the above coordinated water pendants of the double-layers [O8···O7, 2.679(7) Å]. Although some honeycomb structures have been found,[7,14,33] compound **1** is, to the best of our knowledge, unprecedented because of the double-layer conformation.

Compound **2** exhibits a 3D hybrid framework constructed from chains of corner-linked octahedra connected by carboxylate linkers (Figure 2). Each indium atom binds to four carboxylate oxygen atoms from four H_2BTEC groups and two other bridging oxygen atoms (O17 and O18) to form an octahedron. Bond valence calculations for O17 and O18 give a value of 1.3. Thus, the oxygen atoms (O17 and O18) can be considered to be μ-OH functions thereby balancing the negative charge in **2**. The octahedra are linked into infinite chains running along the [010] direction via μ-OH functions. Furthermore, two adjacent octahedra in one chain are bridged by two carboxylate arms from two different organic linkers. The octahedra are severely tilted and this is reflected by angles of 122.1(5)° (In1−O17−In1) and 122.2(5)° (In2−O18−In2), both being very far from the value 180° which would be expected if the chains of octahedra were perfectly linear. Each H_2BTEC group binds to four indium atoms, in a bidentate mode, situated in two different chains through the 1,5-carboxylate arms. The other two carboxylate arms are uncoordinated and protonated. Geometrically, the latter two carboxylate arms are coplanar with the phenyl ring whereas the other two are perpendicular to the phenyl rings. All phenyl rings are perpendicular to the directions of the chains. The chains are interweaved by organic linkers in such a way that the

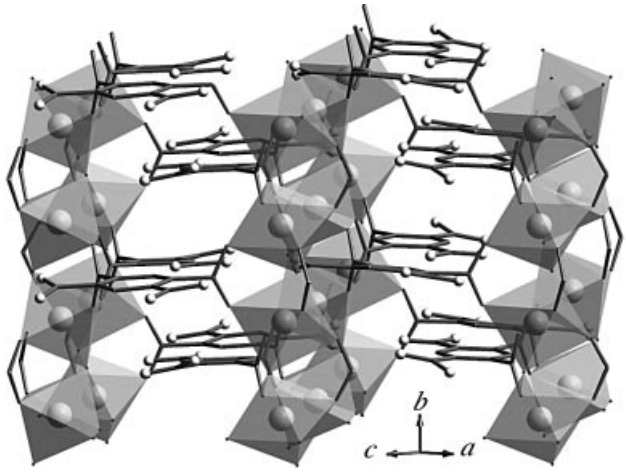

Figure 2. View of the interconnection between polyhedral chains and H_2BTEC groups in **2**; free water oxygen atoms are omitted for clarity

adjacent indium atoms in any chain are situated at approximately $y = 0$ and $y = 1/2$ while the phenyl rings located between two indium atoms are at approximately $y = 1/4$ on one side of the chain and $y = 3/4$ on the other side of the same chain (Figure 3). Such arrangement of metal and organic moieties is similar to that of the compound MIL-61.[28] These types of connections between the organic and inorganic moieties result in 1D polygonal tunnels. However, the uncoordinated carboxylic functions point towards these tunnels and reduce the effective sizes of the cavities. This helps understand why **2** absorbs little nitrogen gas even after dehydration.[31] Water molecules reside in the tunnels and give rise to hydrogen bonds with uncoordinated carboxylic functions [O19···O14 2.65(2) Å, O20···O5 2.629(8) Å, O19···O8A 2.859(4) Å, O20···O12B 2.915(3) Å. Symmetry code: (A) $-x$, $-0.5 + y$, $0.5 - z$; (B) $1 - x$, $1 - y$, $1 - z$].

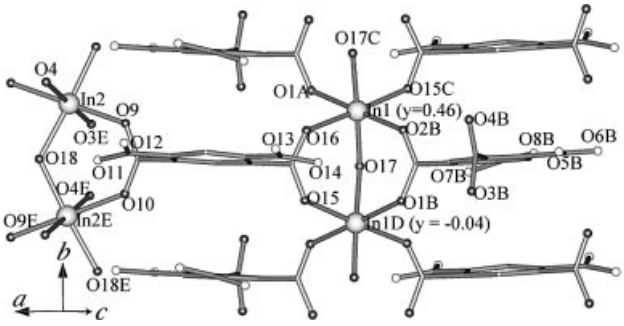

Figure 3. Diagram showing the relative positions of indium atoms and H2BTEC groups in **2**; selected bond lengths (Å): In1−O1A 2.19(1), In1−O2B 2.16(1), In1−O15C 2.18(1), In1−O16 2.20(1), In1−O17 2.00(1), In1−O17C 2.12(1); In2−O3E 2.16(1); In2−O4 2.17(1); In2−O9 2.16(1); In2−O18 2.06(1); In2E−O18 2.07(1); In2E−O10 2.21(1); selected bond angles (°): O1A−In1−O2B 179.3(4); O1A−In1−O16 89.2(5); O16−In1−O2B 91.2(5); O17−In1−O5C 90.0(5); In1−O17−In1D 122.1(5); O3E−In2−O4 178.6(6); O4−In2−O9 89.0(5); In2−O18−In2E 122.2(5); symmetry code: (A) x, $1.5 - y$, $0.5 + z$; (B) $-x$, $1 - y$, $1 - z$; (C) $-x$, $0.5 + y$, $1.5 - z$; (D) $-x$, $-0.5 + y$, $1.5-z$; (E) $1 - x$, $-0.5 + y$, $1.5 - z$

The homogeneous nature of compounds **1** and **2** was shown by X-ray powder diffraction (XRPD) patterns (Figure 4). The powder patterns obtained experimentally for **1** (b) and **2** (e) are in agreement with the calculated patterns for **1** (a) and **2** (d), respectively. The exceptions are the lines at $2\theta = 16.5$ and 20.5° in **2** which are too intense in the experimental pattern. This phenomenon is a result of the preferred orientation of the crystallites.

The infrared absorption bands of **1** and **2** are listed in Table 1. In **1**, the absence of the characteristic bands at 1730−1690 cm^{-1} due to the protonated carboxylate groups indicates that complete deprotonation of H_3BTC occurs upon reaction with indium ions.[34] A strong absorption at 1731 cm^{-1} in **2** confirms the presence of the carboxylic acid function. Both results are in agreement with the crystallographic data.

Thermogravimetric (TG) analyses were carried out under air. The TG diagram (Figure 5) of **1** shows that the first weight loss of 10.1% occurring from about 50 °C to 167 °C

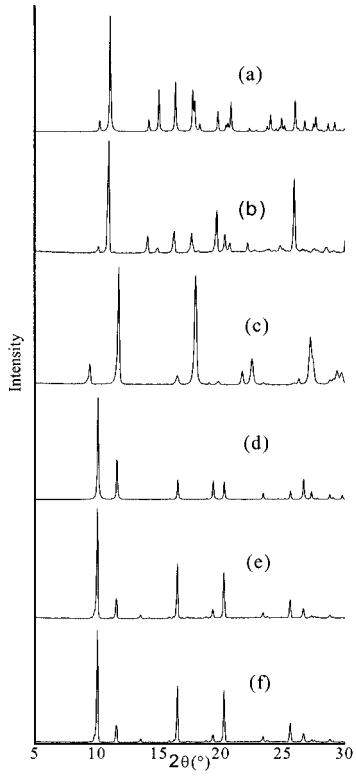

Figure 4. The calculated (a) and experimental (b) XRPD patterns for **1** and the calculated (d) and experimental (e) XRPD patterns for **2**; the patterns (c) and (f) correspond to the sintered samples at 180 °C for **1** and **2**, respectively

Table 1. Characteristic IR absorption bands for **1** and **2** (cm^{-1})

	$\upsilon_{as}(CO_2^-)$	$\upsilon_s(CO_2^-)$	$\upsilon(CO_2H)$	$\upsilon(H_2O)$	$\upsilon(OH)$
1	1619 (s)	1441 (s)		3420 (s)	
	1583 (m)	1384 (s)			
2	1579 (vs)	1444 (s)	1731 (s)	3489 (s)	3127 (s)
	1495 (m)	1400 (vs)			

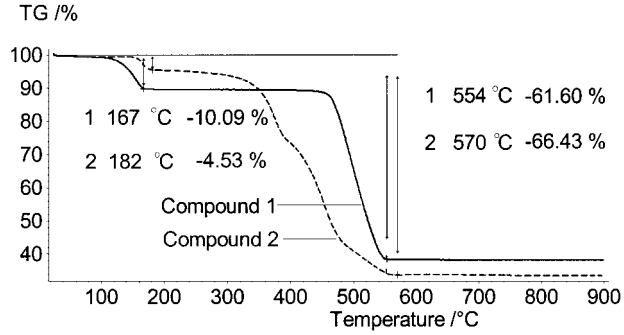

Figure 5. TG curves for **1** and **2**

corresponds to the complete loss of free and coordinated water molecules (calculated: 10.1%), accompanied by the transformation of the framework of **1** indicated by the XRD pattern (see c in Figure 4). The second weight loss, occurring from about 424 °C to 554 °C, is the stage at which **1** dramatically loses its organic component. The light yellow

residue is In_2O_3 with a residual weight fraction of 38.4% (calculated: 38.8%). This was confirmed by XRD analysis.

Compound **2** also undergoes a two-step weight loss (Figure 5). The first weight loss of 4.53% from about 50 °C to 182 °C can be attributed to the loss of free water molecules (calculated: 4.48%). In contrast to compound **1**, XRD studies show that the framework of **2** remains intact after the loss of water molecules (see f in Figure 4). The second weight loss occurs in the temperature range of 380 to 570 °C, in which **2** dramatically loses weight and begins decomposing due to the loss of organic matter. The residue at 570 °C weighing 33.6% of the total is In_2O_3 (calculated: 34.53%). This was confirmed by XRD analysis.

Compounds **1** and **2** exhibit intense greenish-blue emissions in the solid state at 494 nm (λ_{ex} = 325 nm) for **1** and 489 nm (λ_{ex} = 337 nm) for **2**. Compared with the fluorescent analysis of other metal-BTC compounds,[33] we can assign the 494 and 489 nm emission bands to ligand-to-metal charge-transfer (LMCT) processes.

Experimental Section

Synthesis of $[In_2(BTC)_2(H_2O)_2]_n \cdot 2nH_2O$ (1): Compound **1** was synthesised hydrothermally from the reaction of $InCl_3$ (221 mg, 1 mmol), H_3BTC(210 mg, 1 mmol), pyridine (0.3 mL, 3.7 mmol) and H_2O (5 mL) (pH value 2−3) in a 30-mL Teflon-lined stainless steel vessel at 120 °C for 85 h. The reaction mixture was then cooled at a rate of 6 °C·h^{-1} to give the only product, namely colourless crystals of **1**. The crystals were collected and washed with *N*,*N*-dimethylformamide and distilled water. The yield was 85% (302 mg) based on $InCl_3$. Elemental analysis calcd. (found) for $C_9H_7InO_8$ (*fw* = 357.97): calcd. C 30.20 (30.17), H 1.97 (1.93). IR (KBr pellet [cm^{-1}]): $\tilde{\nu}$ = 3420 (vs, br), 3090 (m), 1619 (vs), 1583 (m), 1548 (s), 1441 (vs), 1384 (vs), 1114 (w), 1061 (w), 757 (s), 715 (m).

Synthesis of $[In_2(H_2BTEC)_2(OH)_2]_n \cdot 2nH_2O$ (2): Compound **2** was synthesised hydrothermally from the reaction of $InCl_3$ (221 mg, 1 mmol), pyromellitic dianhydride (218 mg, 1 mmol), pyridine (0.3 mL, 3.7 mmol) and H_2O (6 mL) (pH value = 2−3) in a 30-mL Teflon-lined stainless steel vessel at 160 °C for 85 h. The reaction mixture was then cooled at a rate of 6 °C·h^{-1} to give the only product, namely colourless crystals of **2**. The crystals were collected and washed with *N*,*N*-dimethylformamide and distilled water. The yield was 70% (280 mg) based on $InCl_3$. Elemental analysis calcd. (found) for $C_{20}H_{14}In_2O_{20}$ (*fw* = 803.95): calcd. C 29.88 (30.10), H 1.76 (1.80). IR (KBr pellet [cm^{-1}]): $\tilde{\nu}$ = 3489 (m, br), 3127 (m), 1731 (s), 1579 (vs), 1495 (m), 1444 (s), 1400 (vs), 1345 (m), 1275 (s), 1210 (s), 1047 (m), 796 (m).

Crystallographic Studies: The crystal data and structure determination parameters for **1** and **2** are listed in the Table 2.[35] Intensity data were collected on a Rigaku−Mercury CCD diffractometer with graphite-monochromated Mo-K_α (λ = 0.71073 Å) radiation using the ω-2θ scan method at room temperature. The structures were solved by direct methods and all calculations were performed using the SHELXL-97 PC program. All nonhydrogen atoms were refined anisotropically. All hydrogen atoms were calculated in the ideal positions and refined isotropically. The structures were refined on F^2 using full-matrix least-squares methods.

Table 2. Crystallographic data for **1** and **2**.

	1	**2**
Empirical formula	$C_9H_7InO_8$	$C_{20}H_{14}In_2O_{20}$
Molecular mass	357.97	803.95
Crystal system	monoclinic	monoclinic
Space group	$P2_1/c$	$P2_1/c$
a (Å)	6.9532(7)	18.5774(19)
b (Å)	8.9789(8)	7.2222(0)
c (Å)	17.525(2)	21.4155(15)
β (°)	100.153(6)	125.187(6)
V (Å^3)	1077.0(1)	2348.3(3)
Z	4	4
D_c (g cm^{-3})	2.208	2.274
μ (mm^{-1})	2.228	2.069
Data collection (°)	$2.36 \le \theta \le 25.02$	$1.34 \le \theta \le 25.02$
Reflns. collected	6442	13746
Indep. reflns.	1901	4141
Reflns. with $I > 2\sigma(I)$	1661	3525
$R_{int.}$	0.0339	0.0414
Restrains/parameters	0/163	0/388
$(\Delta\rho)_{max}/(\Delta\rho)_{min}$, e/Å^3	0.804/−0.510	2.481/−3.795
R_1[a] [$I > 2\sigma(I)$]	0.0312	0.0940
wR[b] (all data)	0.0681	0.2344

[a] $R = \Sigma(||F_o| - |F_c||)/\Sigma|F_o|$. [b] $wR = \{\Sigma w[(F_o^2 - F_c^2)^2]/\Sigma w[(F_o^2)^2]\}^{1/2}$.

Acknowledgments

This work was supported by the National Nature Science Foundation of China (No. 20231020) and the Nature Science Foundation of Fujian Province.

[1] K. S. Min, M. P. Suh, *J. Am. Chem. Soc.* **2000**, *122*, 6834−6840.
[2] S. Noro, S. Kitagawa, M. Kondo, K. Seki, *Angew. Chem. Int. Ed.* **2000**, *39*, 2081−2084.
[3] M. Eddaoudi, D. B. Moler, H. Li, B. Chen, T. M. Reineke, M. O′Keeffe, O. M. Yaghi, *Acc. Chem. Res.* **2001**, *34*, 319−330.
[4] B. Moulton, M. J. Zaworotko, *Chem. Rev.* **2001**, *101*, 1629−1658.
[5] M. J. Plater, M. R. S. E. Foreman, C. J. Gomez-Garcia Coronado, A. M. Z. Slawin, *J. Chem. Soc., Dalton Trans.* **1999**, *23*, 4209−4216.
[6] M. Yaghi, H. L. Li, T. L. Groy, *J. Am. Chem. Soc.* **1996**, *118*, 9096−9101.
[7] H. J. Choi, M. P. Suh, *J. Am. Chem. Soc.* **1998**, *120*, 10622−10628.
[8] M. J. Plater, R. A. Howie, A. J. Roberts, *Chem. Commun.* **1997**, 893−894.
[9] C. J. Kepert, T. J. Prior, M. J. Rosseinsky, *J. Solid State Chem.* **2000**, *152*, 261−270.
[10] D. P. Cheng, M. A. Khan, R. P. Houser, *Inorg. Chem.* **2001**, *40*, 6858−6859.
[11] M. P. Suh, J. W. Ko, H. J. Choi, *J. Am. Chem. Soc.* **2002**, *124*, 10976−10977.
[12] T. J. Prior, M. J. Rosseinsky, *Chem. Commun.* **2001**, 1222−1223.
[13] W. Chen, J. Y. Wang, C. Chen, Q. Yue, H. M. Yuan, J. S. Chen, S. N. Wang, *Inorg. Chem.* **2003**, *42*, 944−946.
[14] T. J. Prior, M. J. Rosseinsky, *Chem. Commun.* **2001**, 495−496.
[15] J. R. Su, K. L. Yin, D. J. Xu, *Chin. J. Struct. Chem.* **2004**, *23*, 399−402.
[16] T. J. Prior, M. J. Rosseinsky, *Inorg. Chem.* **2003**, *42*, 1564−1575.
[17] H. Kumagai, C. J. Kepert, M. Kurmoo, *Inorg. Chem.* **2002**, *41*, 3410−3422.
[18] F. D. Rochon, G. Massarweh, *Inorg. Chim. Acta* **2001**, *314*, 163−171.

[19] R. Murugavel, D. Krishnamurthy, M. Sathiyendiran, *Dalton Trans.* **2002**, 34−39.
[20] R. Diniz, H. A. de Abreu, W. B. de Almeida, M. T. C. Sansiviero, N. G. Fernandes, *Eur. J. Inorg. Chem.* **2002**, 1115−1123.
[21] M. Sanselme, J. M. Greneche, M. Riou-Cavellec, G. Ferey, *Chem. Commun.* **2002**, 2172−2173.
[22] D. F. Sun, R. Cao, Y. C. Liang, Q. Shi, M. C. Hong, *Dalton Trans.* **2002**, 1847−1851.
[23] C. D. Wu, C. Z. Lu, W. B. Yang, S. F. Lu, H. H. Zhuang, J. S. Huang, *Eur. J. Inorg. Chem.* **2002**, 797−800.
[24] R. Cao, D. F. Sun, Y. C. Liang, M. C. Hong, K. Tatsumi, Q. Shi, *Inorg. Chem.* **2002**, *41*, 2087−2094.
[25] C. Daiguebonne, O. Guilloa, Y. Gerault, A. Lecerf, K. Boubekeur, *Inorg. Chim. Acta* **1999**, *284*, 139−145.
[26] Z. Z. Lin, J. H. Luo, M. C. Hong, R. H. Wang, L. Han, Y. Xu, R. Cao, *J. Solid State Chem.* **2004**, *177*, 2494−2498.
[27] D. Q. Chu, C. L. Pan, L. M. Wang, J. Q. Xu, *Mendeleev Commun.* **2002**, 207−209.
[28] K. Barthelet, D. Riou, M. Nogues, G. Ferey, *Inorg. Chem.* **2003**, *42*, 1739−1743.
[29] Manuscript in preparation. Crystallographic data for $[In_4(BTC)_3(OH)_4]_n \cdot 3nH_2O \cdot nHpy\cdot n$py: *C*2/*c*, a = 18.664 Å, b = 14.4433 Å, c = 17.573 Å, β = 114.680°, V = 4304.3 Å^3, Z = 4, Dc = 1.916, R_1 = 0.0665, wR = 0.1160.
[30] Manuscript in preparation. Molecular formula may be $[In_3(BTEC)_2(OH)_2]_n \cdot nHpy\cdot n$py.
[31] Nitrogen adsorption and desorption isotherms were measured at 77 K on a Micromeritics ASAP 2010 Micropore Analyser for **1** and **2**. Before the measurements, the samples were degassed at 523 K for 6 hours and then at room temperature for 16 hours. Both title compounds exhibit a type III isotherm, indicating weak adsorption or no adsorption.
[32] N. E. Brese, M. O′keeffe, *Acta Crystallogr., Sect. B* **1991**, *47*, 192.
[33] J. C. Dai, X. T. Wu, Z. Y. Fu, C. P. Cui, S. M. Hu, W. X. Du, L. M. Wu, H. H. Zhang, R. Q. Sun, *Inorg. Chem.* **2002**, *41*, 1391−1396.
[34] L. J. Bellamy, *The Infrared Spectra of Complex Molecules*; Wiley: New York, **1958**.
[35] CCDC-251131 and -251132 contain the supplementary crystallographic data for this paper. These data can be obtained free of charge at www.ccdc.cam.ac.uk/conts/retrieving.html [or from the Cambridge Crystallographic Data Centre, 12 Union Road, Cambridge CB2 1EZ, UK; Fax: +44-1223-336-033; E-mail: deposit@ccdc.cam.ac.uk].

Received July 9, 2004

